Measurement of magnetic field line stochasticity in nonlinearly evolving, nonequilibrium plasmas

Y. Nishimura, J. D. Callen, and C. C. Hegna

Department of Engineering Physics,

University of Wisconsin-Madison, Wisconsin, 53706-1687

In a tokamak plasma, understanding of both the major disruption and the internal disruption (sawtooth oscillation [1]) is crucial for steady state operations. Recent sawtooth experimental results in the Tokamak Fusion Test Reactor (TFTR) [2] have inferred that magnetic field line stochasticity in the vicinity of the $q = 1$ inversion radius plays an important role in rapid changes in the magnetic field structures and resultant thermal transport; the results [2] suggest that the pressure contour and the magnetic flux surface does not coincide during the sawtooth crash.

Conventional MHD simulation results [3] exhibit the magnetic field line stochasticity in terms of the random motions of field lines observed in Poincaré mappings. However, Poincaré mappings are not a convenient tool for measuring stochasticity. Rather it is numerically easier and better quantitatively to measure stochasticity by determining Lyapunov exponents for diverging magnetic field lines. In the presence of Kolmogorov, Arnold, and Moser (KAM) surfaces, radial transport due to thermal transport along the field lines is inhibited, and one obtains a totally different net radial transport [4]. To extract the microscopic magnetic field structure (which is important for net radial global transport), the characteristic Lyapunov exponents must be calculated. Spatial correlation of the magnetic field lines must be calculated as well, to estimate the correlation length. These statistical values are important to model the effect of finite thermal transport along magnetic field lines in a physically consistent manner.

Numerical simulations have been conducted by using the three dimensional nonlinear initial value MHD code FAR [5, 6]. The FAR code is a full spectral code, which is finite differenced in the radial direction and Fourier expanded in poloidal/toroidal harmonics. Parameters used in the calculations shown here are: aspect ratio $\epsilon = 0.25$, Lundquist number $S = 10^5$. The safety factor was taken to be in the range of $0.81 \leq q \leq 2.2$. Toroidal mode numbers were taken up to $1 \leq n \leq 4$ (total of 43 modes). A total of 500 equally spaced mesh points were used in the radial direction. Magnetic field line trajectories have been obtained by using a fourth order Runge-Kutta-Gill method with optimized integration step numbers.

Figures 1(a) to 6(a) show Poincaré plots of field line trajectories in a poloidal cross section. Kadomtsev-type full reconnection can be seen at $t = 1113t_a$ (Fig. 3(a)); this state relaxes back to a nearly concentric flux surface configuration at $t = 1800t_a$ (Fig. 6(a)). In this specific case, $\beta = 1\%$ ($\beta_p = 0.19$) was taken to suppress the effect of the Shafranov shift. In the presence of harmonics, the trajectories form chains of sideband islands exhibiting poloidally mode coupled structures. Due to the nonlinear interaction of the magnetic perturbations of incommensurate helicity, the magnetic field lines become stochastic and the flux surfaces are no longer invariant. Stochasticity generation is prominent inside the $m = 1$ magnetic island separatrix region as compared to the hot core region which survives nearly intact. The stochasticity in the m=1 island region is due to the distortion of the magnetic surfaces inside the $m = 1$ island and the generation of secondary islands [7]. Interestingly, residual stochasticity can be observed outside the $q = 1$ inversion radius, even after the hot core region is pushed out.

Figures 1(b) to 6(b) show the spatial profile of the Lyapunov exponents of field lines (measured for

200 toroidal revolutions) that start at different initial positions on the X axis of Figs. 1(a) to 6(a). These provide quantitative proof of field line stochasticity. Relatively small values suggest the existence of a stable region. Some exponents converge to a finite value after many more revolutions around the torus; they may be simply staying in the vicinity of a KAM surface.

The resultant pressure evolution in the presence of these magnetic field structures has also been investigated. Figure 3(c) shows the pressure contour and Fig. 3(d) shows the radial pressure profile at the time corresponding to Fig. 3(a). The solid line in Fig. 3(d) is obtained by imposing a relatively large parallel thermal diffusion coefficient ($\kappa_{\parallel}/\kappa_{\perp} = 10^5$). The differences in the profiles for the two different $\kappa_{\parallel}/\kappa_{\perp}$ values suggest a relaxation of radial pressure gradients due to the thermal transport along the stochastic magnetic field lines. With higher β simulations, a ballooning mode structure and instability is observed in the final stage of the sawtooth crash. Qualitative investigation of the ballooning instability threshold in the presence of the large m=1 island structures will be presented. This research was supported by United States Department of Energy Grant No. DE-FG02-86ER53218.

References

[1] S. von Goeler, W. Stodiek, and N. Sauthoff, Phys. Rev. Lett. **33**, 1201 (1974).

[2] Y. Nagayama et al., Phys. Plasmas **3**, 2631 (1996); J. D. Callen, B. A. Carreras, and R. D. Stambaugh, Phys. Today **45**, 34 (1992); M. Yamada et al., Phys. Plasmas **1**, 3269 (1994).

[3] A. Aydemir et al., Phys. Fluids B **1**, 774 (1989); W. Park et al., Phys. Fluids B **3**, 507 (1991); H. Baty, J. F. Luciani, and M. N. Bussac, Phys. Fluids B **5**, 1213 (1993).

[4] J. D. Meiss, Rev. Mod. Phys. **64**, 795 (1992); C. C. Hegna and J. D. Callen, Phys. Fluids B **5**, 1804 (1993); A. J. Lichtenberg et al., Nucl. Fusion **32**, 495 (1992).

[5] L. A. Charlton et al., J. Comput. Phys. **86**, 270 (1990).

[6] Y. Nishimura, J. D. Callen, and C. C. Hegna, UW-CPTC-13, August,1997.

[7] Y. Nishimura and M. Azumi, Phys. Plasmas **4**, 2365 (1997).

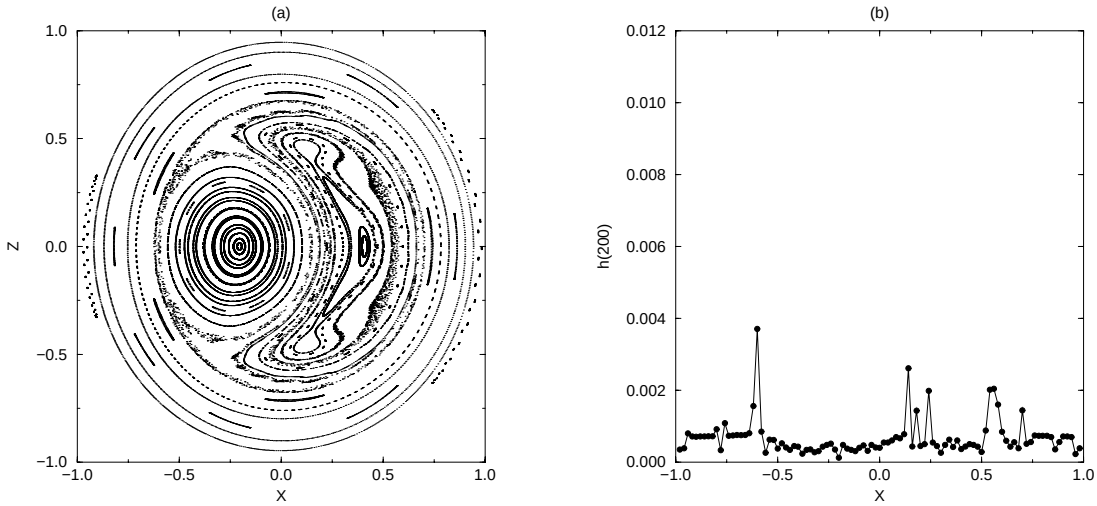

Figure 1: At $t = 1058\tau_a$. (a) Poincaré mappings of magnetic field line trajectories in a poloidal cross section, and (b) spatial profile of Lyapunov exponents after 200 toroidal revolutions.

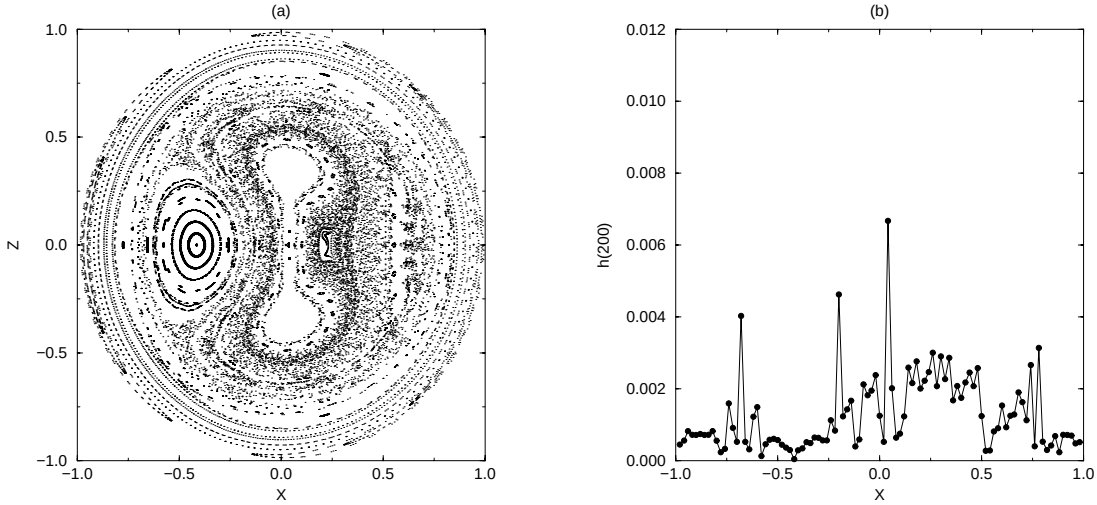

Figure 2: At $t = 1093\tau_a$. (a) Poincaré mappings, and (b) Lyapunov exponents.

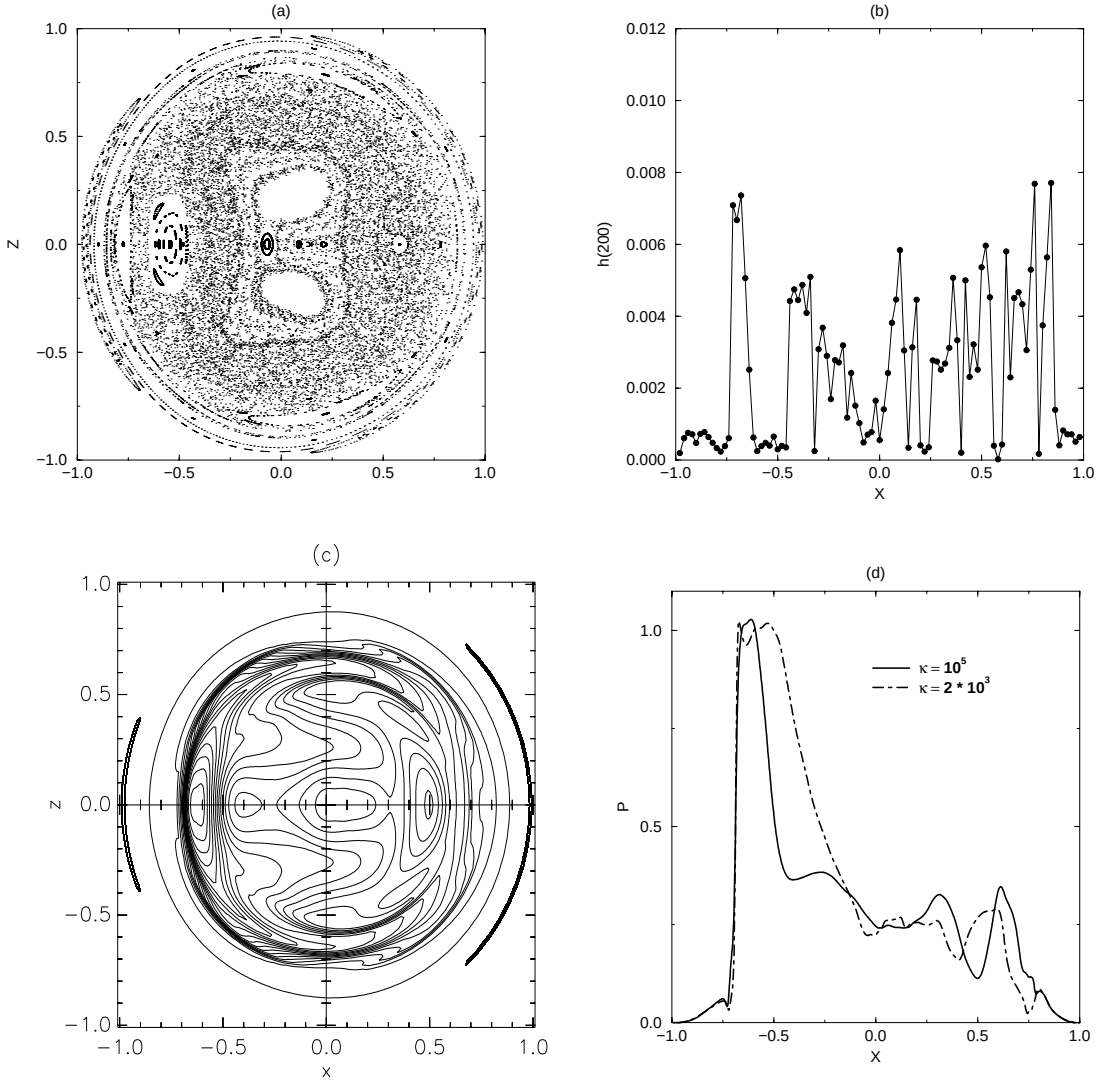

Figure 3: At $t = 1133\tau_a$. (a) Poincaré mappings, (b) Lyapunov exponents, (b) pressure contours, and (d) radial pressure profiles.

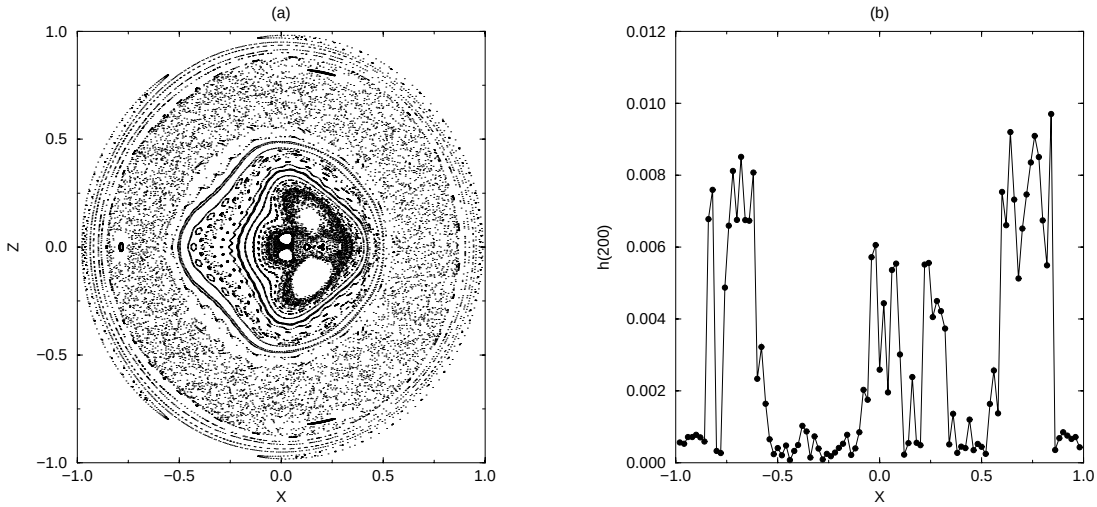

Figure 4: At $t = 1133\tau_a$. (a) Poincaré mappings, and (b) Lyapunov exponents.

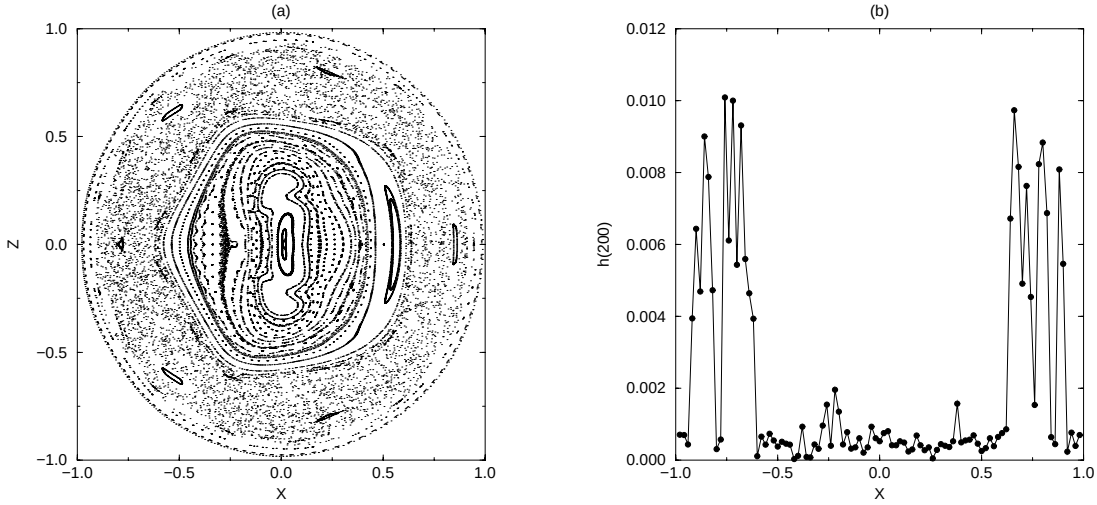

Figure 5: At $t = 1300\tau_a$. (a) Poincaré mappings, and (b) Lyapunov exponents.

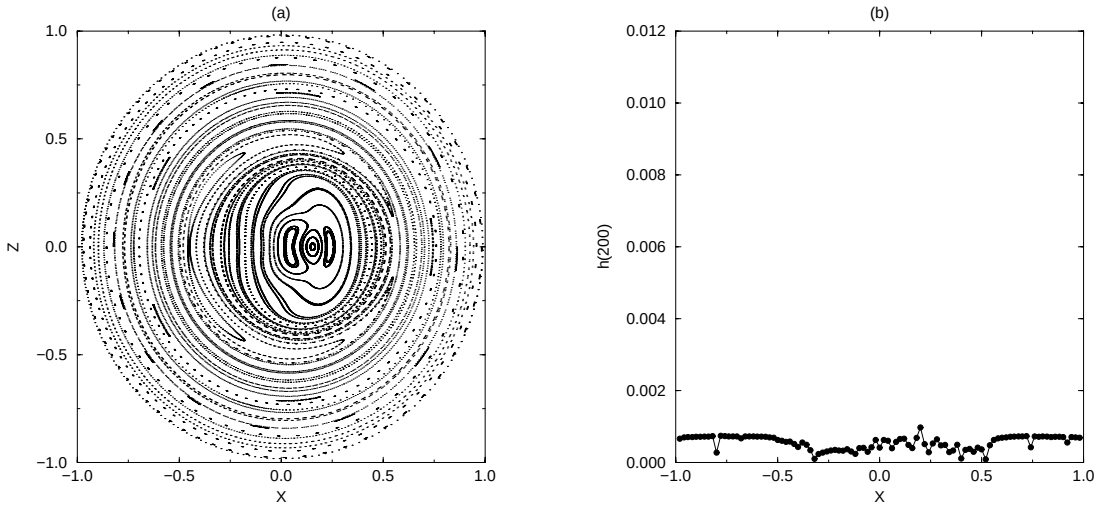

Figure 6: At $t = 1800\tau_a$. (a) Poincaré mappings, and (b) Lyapunov exponents.

Nishimura, Yasutaro
University of Wisconsin-Madison
1500 Engineering Dr.
Madison, WI 53706-1687
Tel: 608-263-0812
Fax: 608-262-6707
email: nishimur@cptc.wisc.edu